

## **Bio-oil upgrading in supercritical water using Ni-Co catalysts supported on carbon nanofibres**

J. Remón<sup>a,b\*</sup>, J. Arauzo<sup>a</sup>, L. García<sup>a</sup>, P. Arcelus-Arrillaga<sup>b</sup>, M. Millan<sup>b\*</sup>, I. Suelves<sup>c</sup>, J.L. Pinilla<sup>c\*</sup>

<sup>a</sup>Thermochemical Processes Group (GPT), Aragón Institute for Engineering Research (I3A), Universidad de Zaragoza. Mariano Esquillor s/n, E-50018 Zaragoza, Spain.

<sup>b</sup>Department of Chemical Engineering, Imperial College London, London SW7 2AZ, United Kingdom

<sup>c</sup>Instituto de Carboquímica, CSIC. Miguel Luesma Castán 4, 50018 Zaragoza, Spain.

\*Corresponding author at University of Zaragoza: e-mail: jrn@unizar.es; phone: +34976762224

\*Corresponding author at Imperial College: e-mail: marcos.millan@imperial.ac.uk; phone: +44(0)2075941633

\*Corresponding author at Instituto de Carboquímica: e-mail: jlpinilla@icb.csic.es; phone: +34976733977

### **ABSTRACT**

This work addresses the preparation, characterisation and screening of different Ni-Co catalysts supported on carbon nanofibres (CNFs) for use in the upgrading of bio-oil in supercritical water. The aim is to improve the physicochemical properties of bio-oil so that it can be used as a fuel. The CNFs were firstly oxidised in HNO<sub>3</sub> and afterwards subjected to a thermal treatment to selectively modify their surface chemistry prior to the incorporation of the metal active phase (Ni-Co). The CNFs and the supported catalysts were thoroughly characterised by several techniques, which allowed a relationship to be established between the catalyst properties and the upgrading results. The use of Ni-Co/CNFs for bio-oil upgrading in supercritical water (SCW) significantly improved the properties of the original feedstock. In addition, the thermal treatment to which the fibres were subjected exerted a significant influence on their catalytic properties. An increase in the severity of the thermal treatment led to a substantial reduction in the oxygen content of the CNFs, mainly due to the removal of the less

stable oxygen surface groups, which allowed their surface polarity to decrease. This decrease resulted in less formation of solid products. However, it also reduced the H/C and increased the O/C ratios of the upgraded liquid. Therefore, a compromise between the yield and the properties of the upgraded bio-oil was achieved with a Ni-Co supported on a CNF with a moderate amount of oxygen surface groups.

**Keywords:** bio-oil upgrading, supercritical water, bio-fuels, carbon nanofibres

## **1. Introduction**

The increase in the worldwide energy demand, which in 2050 is likely to be double what it was in the year 2000 [1, 2], along with declining resources have led investigators to seek alternative technologies, materials and more sustainable strategies to produce energy, fuels and chemicals. Under this new energetic scenario, the development of new processes and the employment of renewable materials to achieve an environmentally friendly production of energy and chemicals are of paramount importance to satisfy the energy consumption requirements of the present petroleum-based society and the well being of the generations of the future. In this context, the use of biomass as a renewable feedstock to cope with the energetic issues of the current market is gaining increasing attention [3]. Among the different processes for biomass valorisation, fast pyrolysis is the most mature and industrially used technology. This process is able to transform this solid feedstock into a liquid product (bio-oil) that could be further used for the production of chemicals and energy towards a greener and more environmentally friendly chemistry.

Lignocellulosic bio-oils contain the degradation products of biomass (cellulose, hemicellulose and lignin [4]) and are made up of a mixture of different organic compounds [5] with different chemical compositions depending on the pyrolysis step [6]. These bio-oils are promising source for liquid bio-fuels [4, 7, 8]. However, some of the properties of these liquids (elevated viscosity, high O/C ratio, large H<sub>2</sub>O content and low pH) hinder their direct use as liquid biofuels [9]. This scenario makes the upgrading of bio-oil an essential challenge in order to obtain liquid biofuels from biomass and several processes such as hydrotreating, hydrocracking and the use of supercritical water [4, 7, 8, 10] have been developed and tested to achieve this goal.

Among these different upgrading technologies, the use of supercritical water (SCW) is emerging as a promising alternative for bio-oil valorisation [11], as it enables an upgraded liquid biofuel to be obtained [10]. However the works dealing with lignocellulosic bio-oil upgrading in supercritical water are extremely scarce and are focused on gas production rather than liquid bio-fuels. This latter indicates that more insight should be gained for the scale-up and commercialisation of this emerging technology. Specifically, Penninger and Rep [12] analysed the supercritical water reforming of bio-oil for H<sub>2</sub> production, while Onwudili and Williams [13] studied the supercritical water gasification for the production of CH<sub>4</sub>. Remón et al. [10] investigated the use of water in sub- and supercritical state for bio-oil valorisation using a Ni catalyst supported on alumina prepared by coprecipitation (Ni-Co/Al-Mg). The effects of the water regime (sub- and supercritical) and the most important operating conditions on the process were reported.

In addition, the design of catalysts for the SCW upgrading of bio-oil is of paramount importance for the development and expansion of this technology. The catalysts should strike a compromise between activity, selectivity and stability. In particular, the selection of a stable support that can withstand the supercritical conditions constitutes a challenge due to lack of stability in the presence of hot compressed water [14, 15]. Moreover, the acidic nature of some supports, such as the commonly used  $\gamma$ -Al<sub>2</sub>O<sub>3</sub>, is known to cause substantial coke deposition and rapid catalyst deactivation.

These drawbacks have prompted the investigation of novel non-acidic catalytic supports. In particular, nanofilamentous carbon (NC) aggregates, such as carbon nanofibres (CNF) and carbon nanotubes (CNT), are considered promising catalyst supports for liquid phase reactions due to their high chemical stability in non-oxidizing environments, their tuneable chemical nature and their outstanding textural properties [16, 17]. The stability of CNF in supercritical water has recently been assessed [18]. The NC structure is an inverse copy of a conventional support, with the spaces between the filaments serving as pores and the metal sites anchoring to the nanofilament walls [19]. This open structure facilitates the diffusion of reactants and products by reducing steric hindrance. As regards their tuneable chemical nature, it is relatively easy to modify the surface chemistry of NC by, for instance, attaching oxygen surface groups that may have an impact not only on the active phase morphology but also on the catalyst activity [20-22]. The material thus constitutes a very promising support for use in various catalytic processes.

In this context, CNFs have been used in many different processes. These include the

hydrogenation of light alkenes [23-27], aldehydes [21, 28-33], polycyclic aromatic hydrocarbons [34], nitrobenzene [35], and cyclohexene [36]. They have also been used in alkene hydroformylation [37], vacuum residue hydroprocessing [38, 39], ammonia and Fisher-Tropsch synthesis [40-42], cyclohexanol dehydrogenation [43], NO decomposition [44] and aniline oxidation [45, 46]. However, CNFs have not been applied to bio-oil upgrading in supercritical water and more research is needed to develop suitable catalysts for this upgrading technology.

Given this scenario, this work addresses the use of CNFs for catalytic upgrading of lignocellulosic bio-oil in supercritical water, aiming to produce an upgraded liquid with improved physicochemical properties which may be used as a fuel. Three different Ni-Co catalysts supported on CNFs were prepared. The CNFs were firstly oxidized in HNO<sub>3</sub> and subsequently subjected to a thermal treatment at 600 and 900 °C, aiming to reduce the amount of oxygen surface groups to decrease the polarity of the support. They were then tested for bio-oil upgrading in SCW. Owing to the high number of different compounds with different polarities present in the bio-oil, the modification of the polarity of the support will have an effect on this upgrading process and alter the properties of the upgraded liquid. This study provides the first report on the use of CNFs for bio-oil upgrading in supercritical water. A thorough characterisation of the catalysts was performed in order to establish a relationship between catalyst properties and extent of bio-oil upgrading.

## 2. Experimental

### 2.1 Bio-oil characterisation

Biomass Technology Group (BTG) in the Netherlands supplied the bio-oil used in this work. It was produced during the pyrolysis of pine sawdust using a rotating cone reactor. The most important properties of the original liquid are summarised in Table 1. Further information about the methodology and apparatus used for the characterisation of the bio-oil can be found in a previous communication [10]. An empirical correlation developed by Channiwala and Parikh [47] was used for estimating the HHV of the treated liquids due to the small amount of sample obtained in each experiment. This experimental correlation was validated experimentally [10]. The original bio-oil and the treated liquid were analysed by GC-MS [10].

### 2.2 CNF synthesis and functionalisation

Fishbone-like CNF were produced by the catalytic decomposition of a mixture of  $\text{CH}_4:\text{CO}_2$  (1:1) in a rotary bed reactor described elsewhere [48] using a  $\text{Ni}/\text{Al}_2\text{O}_3$  catalyst. The syntheses were carried out at 600 °C and a weight hourly space velocity of  $30 \text{ L}\cdot(\text{g}_{\text{cat}}\cdot\text{h})^{-1}$ . More details about the CNF synthesis and functionalization can be found in [34]. The CNF were functionalised with concentrated  $\text{HNO}_3$  (65 wt.%) at boiling temperature for 30 min (denoted as  $\text{CNF}_f$ ). Typically, 10 g of CNF were refluxed in 250 mL of acid solution. The  $\text{CNF}_f$  were filtered and washed with distillate water until the pH of the filtrate was above 6. Finally, the materials were dried overnight at 80 °C. Afterwards, a thermal treatment under a  $\text{N}_2$  flow at either 600 or 900 °C was carried out

in order to selectively modify the amount of the oxygen surface groups. These samples are denoted as CNF<sub>F</sub>-600 or CNF<sub>F</sub>-900.

### *2.3 Catalyst preparation*

Catalysts were prepared using the coprecipitation method previously reported [49]. Briefly, a solution of NH<sub>4</sub>OH was added to an aqueous solution of the respective nitrates (Ni(NO<sub>3</sub>)<sub>2</sub>·6H<sub>2</sub>O and Co(NO<sub>3</sub>)<sub>2</sub>·6H<sub>2</sub>O) and the CNF supports until a pH of 8.2 was reached, aiming to achieve a composition of 19 wt.% Ni and 2.5 wt.% Co. The precipitation medium was maintained at 40 °C and moderately stirred during 30 minutes. The catalyst precursors were filtered and washed with distillate water until the pH of the filtrate was above 6 and subsequently dried overnight at 108 °C. Afterwards, approximately 1 g of catalyst was placed in a quartz tube inside a tubular furnace. A tempering treatment aimed to decompose the metal precursor salts was carried out by flowing N<sub>2</sub> at 50 mL·min<sup>-1</sup> for 1 h at 450 °C followed by a reduction step at the same temperature under a H<sub>2</sub> flow of 50 mL·min<sup>-1</sup> for 2 hours. The catalysts were passivated with an O<sub>2</sub> (1 vol.%) / N<sub>2</sub> flow in the same reactor at room temperature during 12 h to prevent re-oxidation upon contact with air. The catalysts are denoted as NiCo/CNF<sub>F</sub>, NiCo/CNF<sub>F</sub>-600 and NiCo/CNF<sub>F</sub>-900.

### *2.4 Solid characterisation*

The amounts of Ni and Co deposited on the CNF were estimated using ICP-OES analysis (Jobin Yvon 2000). A PAN analytical diffractometer equipped with a Ni-filtered Cu K $\alpha$  radiation and a secondary graphite monochromator ( $\theta$ -2 $\theta$  configuration)

was used to acquire the Powder X-ray diffraction (XRD) patterns of the samples. TEM images were taken with a Jeol 2011 microscope equipped with a LaB<sub>6</sub> gun operating at 200 kV. A drop of a solution of finely ground sample dispersed in ethanol was deposited on a standard TEM copper grid, previously covered by a lacey amorphous carbon film.

The amount of surface oxygen groups created during the functionalisation treatments on the CNF was determined by Temperature Programmed Desorption (TPD) measurements using an AutoChem II 2920 apparatus. X-ray photoelectron spectroscopy (XPS) analyses were carried out with an ESCA Plus OMICROM system equipped with a hemispherical electron energy analyser. More details about the methodology used in TPD and XPS analysis can be found elsewhere [34].

### *2.5 Experimental system and procedure for bio-oil upgrading*

The upgrading experiments were conducted in a stainless steel micro-bomb batch reactor. The reactor consists of two sections, a reaction section and a gas recovery section, isolated one from the other with a heavy duty high T and high P needle valve with grafoil seal. The reaction section has a volume of 12 mL and is comprised of a ½ inch Swagelok bored-through tee with two ends plugged. The tee is connected by means of a ¼ inch tube with a wall thickness of 0.069 inches to the high T and high P needle valve. The gas product recovery section is equipped with a pressure gauge to determine the pressure of the gas produced after reaction and with an integrated septum that enables the sampling of gas for analysis. A detailed diagram of the reactor is shown in

Fig. 1. The design and operation of this reactor have been presented elsewhere [10, 50]. Briefly, the tee was loaded with the required amount of bio-oil, water and catalyst before attaching it to the rest of the reactor. Then the system was leak tested and purged with helium to ensure an oxygen free atmosphere to start the experiment. The experiments were performed at a temperature of 380 °C and a pressure of 230 bar using a catalyst/dry bio-oil weight ratio of 0.25. After the reaction time was completed the system was quenched in a chilled water bath to stop the reaction. The gas, liquid (upgraded bio-oil) and solid products were recovered, measured and characterised following the experimental procedure described in a previous communication [10]. Briefly, the liquid product was recovered by rinsing the reactor with chloroform to recover the organic and aqueous products. This liquid phase was then filtered with Whatman 1 µm membrane filters (PTFE supported) to separate the solid fraction (spent catalyst, coke and char). The organic and aqueous phases were then separated through decantation. Afterwards, the organic fraction was dried under N<sub>2</sub> flow to determine the amount of bio-oil recovered. The solid fraction was dried overnight at room temperature. Total Organic Carbon (TOC) determined the amount of C in the water phase and values lower than 100 ppm were obtained in all the cases. The solid yield was calculated by difference between the solid fraction and the initial amount of catalyst loaded in the reactor.

### *2.6 Response variables and experimental data processing*

The performance of the different catalysts (NiCo/CNF<sub>f</sub>, NiCo/CNF<sub>f</sub>-600 and NiCo/CNF<sub>f</sub>-900) for bio-oil upgrading in supercritical water was tested by evaluating and comparing their catalytic activity using different response variables (Table 2).

These include the gas, liquid (upgraded bio-oil) and solid yields (%) together with the compositions of the gas (vol.%) and the chemical (relative chromatographic area, %) and elemental (wt.%) compositions of the upgraded liquid product. One-way analysis of variance (one-way ANOVA) with the multiple range least significant difference (LSD) test, both with a significance level of 0.05, were used to evaluate the influence of the CNFs on the process.

### **3. Results and discussion**

#### *3.1 Characterisation of the supports*

Fig. 2 shows a typical TEM micrograph of the as-produced fishbone-like CNF. These tubular structures possess a high aspect ratio and diameter of ca. 50 nm diameter, and they are characterized by an arrangement of the graphitic planes with an inclination of about 30° with respect to the fibre axis. As-prepared CNFs were subjected to a functionalization treatment with HNO<sub>3</sub> at boiling temperature (CNF<sub>f</sub>), which is known to increase the amount of oxygen surface groups without modifying the morphology of the CNF, as previously reported [38]. XRD diffractograms of the CNF<sub>f</sub> (figures not shown) showed the typical prominent reflexion at ca. 26° and a weak peak at ca. 43°, both assigned to graphitic carbon (crystallographic planes (002) and (100), respectively), with  $d_{002}$  and  $L_c$  values of 6.3 nm and 0.3409 nm, respectively (Table 3). After thermal treatment under inert atmosphere (samples CNF<sub>f</sub>-600 and CNF<sub>f</sub>-900), no significant changes in the crystallographic properties took place, as evidenced from the values shown in Table 3. Table 3 also shows the textural properties of the three CNF supports determined by N<sub>2</sub> adsorption. Specific surface area in CNF aggregates is commonly associated to the external surface area while pore volume is ascribed to the space between the nanofibres [51]. No significant differences were observed in the

specific surface area, pore volume or average pore diameter after thermal treatments, and in all cases the samples showed a mesoporous character ( $N_2$  isotherms not shown), typical of this type of material.

The oxygen content determined by TPD is displayed in Table 4. As expected, the amount of oxygen in the  $CNF_f$  sample was relatively high as a result of the functionalization treatment with  $HNO_3$ . The increase in the severity of the thermal treatment (samples  $CNF_{f-600}$  and  $CNF_{f-900}$ ) led to a substantial reduction in the oxygen content mainly due to the removal of the less stable oxygen surface groups, as inferred from the amount of CO and  $CO_2$  released during the TPD experiments (see Fig. 3). The nature of the surface oxygen groups can be assessed as a function of the desorption temperature. Thus,  $CO_2$  desorbed as acidic groups into carboxylic acids (200 °C), carboxylic anhydrides (350 °C) and lactones (600 °C). On the other hand, CO is released as basic and neutral groups such as carboxylic anhydrides (450 °C), phenols and ethers (700 °C) and quinones/carbonyls (900 °C) [52]. Thermal treatment at 600 °C almost completely removed carboxylic acids, anhydrides and lactones, and partially removed phenols and ethers, some of which remained in the carbon surface groups in the form of quinones/carbonyls. After treatment at 900 °C, only the more stable oxygen groups remained on the carbon surface in the form of quinones/carbonyls and to a much lesser extent in the form of phenols. It is clear that thermal treatments allow the polarity of the surface to be adjusted.

Table 4 also shows the decrease in the surface oxygen content and the decrease in the surface O/C ratio (both determined by XPS) as the treatment temperature increases, in

agreement with the TPD results. The relatively high oxygen concentration determined by XPS even in the samples thermally treated at 900 °C can be explained by reoxidation of the sample upon contact with air or to the presence of oxygen groups strongly bonded that are not released upon heating.

### *3.2 Characterisation of the catalysts*

CNF supported catalysts presented very slight variations in textural properties values, as shown in Table 5, confirming that the mesoporous nature of the samples was maintained after metal impregnation. Table 5 shows the metal content of the three catalysts as determined by ICP. The measured metal concentrations were in good agreement with the targeted concentrations. There were no statistically significant differences between the CNFs in amount of Ni and Co incorporated, with 95% confidence. TEM micrographs of the reduced catalysts (Fig. 4) revealed in all cases the presence of nanoparticles of ca. 20 nm average diameter with a standard deviation of ca. 10 nm well dispersed on the CNFs. The insets in Fig. 4 show the nanoparticle size distribution of over 400 particles, revealing little difference between the catalysts. This implies that the surface chemistry of the carbon supports did not have an impact on the nanoparticle size distribution. EDX analysis of some representative single nanoparticles showed that they are composed of Ni and Co (an example of an EDX analysis of a single nanoparticle in the NiCo/CNF<sub>f</sub> catalyst is shown in Fig. 4d) and the average ratio of the amount of Ni to Co in these particles is similar to that measured by ICP. This confirms the formation of bimetallic nanoparticles on the carbon supports.

Fig. 5 shows the XRD patterns of the catalysts. Besides the peak at ca.  $26^\circ$ , associated to graphitic carbon, three sharp diffraction peaks at  $2\theta$  values of  $44.5^\circ$ ,  $51.8^\circ$  and  $76.3^\circ$  were observed in the three samples. These reflexions are commonly assigned to crystallographic planes of face-centred cubic metallic Ni (111), (200) and (220), respectively. The diffraction peaks of Ni and Co are obtained at almost the same diffraction angles; therefore XRD cannot be used to distinguish between these two metals [49]. The crystal domain size of the NiCo nanoparticles, as calculated by fitting the peak profiles with a pseudo-Voigt function, was around 21 nm and no significant differences were observed between the catalysts (Table 5). This is consistent with the TEM measurements. Besides this, no signals associated to oxidised nickel species were found in the diffractograms, which provides evidence of the complete reduction of the reducible active phase of the catalysts under the conditions used.

The XPS spectra of the  $\text{Ni}_{2p}$  region revealed the presence of nickel with different oxidation states (Fig. 6a). The peak found at ca. 853.2 eV can be assigned to the binding energy of the  $2p_{3/2}$  for metal Ni with a strong interaction with the carbon support, as previously reported for similar systems based on Ni nanoparticles supported on carbonaceous materials [53, 54]. It presents a slight positive shift of the binding energy as compared to fully reduced elemental nickel (852.8 eV), assigned to a nickel phase richer in electron density, probably a mixture of elemental nickel and carbide species in the form of NiC or  $\text{Ni}_3\text{C}$ . The peak occurring at 856.3 eV corresponds to oxidized nickel, with the corresponding shake-up satellite lines at about 6 eV from the main peak. This signal can be attributed to a protective coating present on the uppermost layers of the nanoparticles, formed during the passivation step carried out immediately after the reduction treatment under  $\text{O}_2$  (1 vol.%) /  $\text{N}_2$  flow at room temperature. This

protective layer formed on the nickel particles prevented the Ni bulk oxidation upon contact with air.

The XPS spectrum of  $\text{Co}_{2p}$  (Fig. 6b) shows a binding energy peak of 778.7 eV, which is slightly higher than the binding energy assigned to metallic Co (787.2 eV, [55]). This positive shift may account for the interaction between Ni and Co forming bimetallic nanoparticles. A broad signal at 781.8 eV corresponding to oxidised forms of Co [56] was also observed. As previously mentioned, this may have originated from the passivation step.

The role of the surface oxygen groups in the morphology of the deposited metallic phase largely depends on the metal precursor and the catalyst preparation method [57, 58]. In this work, the characterisation results indicate that the surface chemistry did not have a significant impact on the Ni-Co nanoparticle morphology, as determined by the TEM, XRD and XPS studies, which permits assessing the effect of the CNF support without any interference of the morphology of the active phase (Ni-Co). This will be shown in the next section.

### *3.3 Supercritical water upgrading*

The catalytic activity of the NiCo/CNF catalysts was tested in the upgrading of bio-oil in supercritical water. The performance of the catalysts has been compared with a blank test in the absence of catalyst to investigate the catalytic activity of the fibres. These

experiments also aimed at elucidating to what extent the modification of the CNF supports by thermal treatment affects the process. Properties of the treated liquid (upgraded bio-oil) obtained with the CNFs and in the blank test have been compared with those of the original bio-oil, when possible. All these results are presented and discussed in sections 3.3.1-3.3.3.

### *3.3.1 Yields to gas, liquid and solid*

Table 6 lists the yields to gas, liquid (upgraded bio-oil) and solid obtained in the experiments. The statistical analysis indicates that the use of NiCo/CNF catalysts exerted a statistically significant influence on the global product distribution. The NiCo/CNF catalysts increased the liquid yield and reduced the formation of gas in comparison with the results obtained in the absence of catalyst. As regards the formation of solids, the solid yield increased with the use of catalyst due to the promotion of cracking and recombination reactions of bio-oil derived products on the catalyst surface to form coke. The vast majority of this solid was the consequence of char formation. Comparison between the catalytic runs illustrates that the modification of the surface chemistry of the supports did not influence the amount of gas produced. Conversely, it had a moderate impact on the yield to liquid. An increase in the temperature at which the CNF supports were treated resulted in an increase in the liquid fraction yield at the expense of the solid fraction. This is due to the larger removal of oxygen groups reducing the support polarity, which in turn decreased the cracking activity of the catalyst, leading to less carbon formation.

### *3.3.2 Gas phase properties*

The gas phase is composed of a mixture of H<sub>2</sub>, CO<sub>2</sub>, CO and CH<sub>4</sub>. The volumetric compositions and the lower heating values (LHVs) of the gas obtained are shown in Table 7. Statistical analysis indicated that the catalyst does not significantly influence the volumetric composition of the gas, with 95% confidence. This seems to indicate that the gas composition might be governed by equilibrium. As a result, the LHV of the gas was also unaffected.

### *3.3.3 Liquid phase properties*

Tables 8 and 9 summarise the most important physicochemical properties of the treated liquids. Table 8 reveals significant differences for the concentrations of C, H and O in the treated liquids with respect to the untreated bio-oil. The comparison between the elemental composition of the original bio-oil and the compositions of the treated liquids shows how the use of supercritical water significantly increases the concentrations of C and H and reduces the proportion of O in the treated bio-oil. These variations led to a significant increase in the HHV of the liquids, which is of paramount importance for the use of bio-oil as a potential substitute for liquid fuels. The use of SCW promotes deoxygenation (decarboxylation and decarbonylation) reactions in near critical and supercritical water [10, 59-61], which accounts for the evolution in the elemental compositions of the treated liquid. Sulphur is one of the major pollutants in biofuels as its presence conduct to SO<sub>x</sub> emissions during combustion. Very interestingly, the level of S in the treated liquid decreases with respect to the original bio-oil. This is in good accordance with other authors [60-62], who have reported that the supercritical water treatment alone (without catalyst) can provide desulphurisation of crude bio-oil.

However, significant variations between catalytic and non-catalytic runs were not detected for the amount of S in the liquids.

The effect of the catalyst on the process can be followed comparing the H/C and O/C ratios of the liquids calculated from the elemental analyses, listed in Table 8. These calculations show that supercritical upgrading significantly increased the H/C and reduced the O/C ratios, with the NiCo/CNF<sub>f</sub> catalyst providing the larger differences respect to the original bio-oil. This positive effect has been reported for other catalysts based on Ni [10, 63] and on other metals [11, 59, 60]. The reduction of the O/C ratio is one of the key aspects for using bio-oil as a liquid fuel [9], and it contributed to a higher HHV than the original bio-oil. A lower O/C is also likely to improve the stability of this feedstock as well as to reducing its high acidity and therefore its corrosiveness.

An increase in the support thermal treatment temperature reduced the H/C ratio of the upgraded bio-oil while increasing its O/C ratio and the yield to liquid, reflecting a loss in catalytic activity. As a consequence of the lower H/C and higher O/C ratio, the HHV of the upgraded bio-oil decreased as the treatment temperature of the supports increased. As mentioned above, thermal treatment at 900 °C decreases the polarity of the support, thus hindering cracking reactions. This may be due to a combination of a lower affinity of the carbon surface towards the oxygen-containing components of the bio-oil and a lower activation of the bio-oil compounds as the surface oxygen groups become more stable. As the treatment at higher temperature led to less formation of solids but higher O/C and lower H/C ratio in the liquid, it is necessary to strike a compromise between liquid yield and physicochemical properties of the upgraded bio-

oil. This highlights the impact of CNF thermal treatment on the SCW upgrading process.

The chemical compositions of the bio-oils were determined and compared. The total amount of compounds that can be identified by GC-MS usually represents about 20 to 22 wt.% of the crude bio-oils [5], as many lignin-derived compounds cannot be analysed due to their high molecular masses. However, useful trends can be retrieved from this analysis, and a comparison can be established between the original bio-oil and the upgraded liquids. Table 9 lists the main families of compounds that are present in the upgraded liquid: hydrocarbons, alcohols, carboxylic acids, ketones, phenols, furans and cyclic compounds. The presence of these compounds is consistent with the results reported by Onwudili and Williams [13] and Remón et. al [10].

The statistical analysis revealed significant differences between the relative amounts of carboxylic acids, phenols and cyclic compounds. Conversely, variations in the concentrations for hydrocarbons, alcohols, ketones and furans were not significant with 95% confidence. The comparison between the chemical compositions of the original bio-oil with the treated liquids showed that the proportion of carboxylic acids in the liquid decreased and the concentrations of phenolic and cyclic compounds increased during the upgrading process. Aromatics, furans and cyclic compounds are less likely to evolve towards reforming than light oxygenated compounds due to the stronger C-C bonds involved as previously reported by Fisk et al. [11].

The decrease in the proportion of carboxylic acids and the increase in the relative amount of phenols occurred with and without catalyst. The reduction in the proportion of carboxylic acids in the treated liquid is beneficial for the use of bio-oil and is consistent with the reaction pathway proposed by Fisk et al. [11]. The high reactivity of carboxylic acids towards gas formation also occurred in the absence of catalyst due to the acidity of the bio-oil [11, 64]. Depolymerisation of the lignin fraction present in the bio-oil yielding alkyl phenols [65] may explain the increase in the proportion of methoxy phenolic compounds in the upgraded liquid in comparison with the original feedstock. These phenols are relatively stable respect to their transformation to gases [11]. The increase in the relative amount of cyclic compounds only took place when using the CNF without thermal treatment and the CNF treated at 600 °C (CNF<sub>r</sub>-600).

#### **4. Conclusions**

Three different Ni-Co catalysts supported on carbon nanofibres were prepared, characterised and tested for bio-oil upgrading in supercritical water. The role of the CNF support, which was subjected to a thermal treatment in order to modify their surface chemistry prior to the incorporation of the metal active phase (Ni-Co), has been studied. An increase in the severity of the thermal treatment led to a substantial reduction of the oxygen content of the CNFs due to the removal of the less stable oxygen surface groups. This allowed the surface of the fibres to become less polar.

The SCW treatment improved the physicochemical properties of the bio-oil. It increased the H/C ratio and HHV and decreased the O/C ratio of the treated liquid with respect to the original feedstock. As a result, an upgraded liquid with a lower proportion of

carboxylic acids and higher concentrations of phenols and cyclic compounds was obtained. The comparison between the results obtained with the CNFs revealed the paramount role of the oxygen surface chemistry of the carbon support in the catalyst performance. An increase in the temperature of the CNF thermal treatment from 600 to 900 °C decreased the polarity of the CNFs, diminishing the cracking activity of the catalyst and the formation of solids. However, thermal treatment of the CNF at the higher temperature also reduced the H/C and increased the O/C ratios of the upgraded bio-oil, showing there is a balance to be achieved between yield and properties of the upgraded bio-oil.

### **Acknowledgements**

The authors wish to express their gratitude to the Aragon Government (GPT group), the European Social Fund and the Spanish MINECO (projects ENE2010-18985, ENE 2011-28318, ENE2013-41523-R and ENE2014-52189-C2-1-R) for providing financial support. Javier Remón Núñez would like to express his gratitude to the Spanish MINECO for the FPI (BES- 2011-044856) and mobility (EEBB-I-14-08688) grants awarded. Jose Luis Pinilla thanks the Spanish MINECO for his Ramon y Cajal research contract.

### **References**

- [1] D.A. Bulushev, J.R.H. Ross, Catalysis for conversion of biomass to fuels via pyrolysis and gasification: A review, *Catalysis Today*, 171 (2011) 1-13.
- [2] J.C. Escobar, E.S. Lora, O.J. Venturini, E.E. Yáñez, E.F. Castillo, O. Almazan, Biofuels: Environment, technology and food security, *Renewable and Sustainable Energy Reviews*, 13 1275-1287.
- [3] D. Ayhan, Biofuels sources, biofuel policy, biofuel economy and global biofuel projections, *Energy Conversion and Management*, 49 (2008) 2106-2116.

- [4] S. Ayalur Chattanathan, S. Adhikari, N. Abdoulmoumine, A review on current status of hydrogen production from bio-oil, *Renewable and Sustainable Energy Reviews*, 16 (2012) 2366-2372.
- [5] K. Sipilä, E. Kuoppala, L. Fagernas, A. Oasmaa, Characterization of biomass-based flash pyrolysis oils, *Biomass and Bioenergy*, 14 (1998) 103-113.
- [6] R. Trane, S. Dahl, M.S. Skjøth-Rasmussen, A.D. Jensen, Catalytic steam reforming of bio-oil, *International Journal of Hydrogen Energy*, 37 (2012) 6447-6472.
- [7] K. Jacobson, K.C. Maheria, A. Kumar Dalai, Bio-oil valorization: A review, *Renewable and Sustainable Energy Reviews*, 23 (2013) 91-106.
- [8] S. Xiu, A. Shahbazi, Bio-oil production and upgrading research: A review, *Renewable and Sustainable Energy Reviews*, 16 (2012) 4406-4414.
- [9] Q. Lu, W.-Z. Li, X.-F. Zhu, Overview of fuel properties of biomass fast pyrolysis oils, *Energy Conversion and Management*, 50 (2009) 1376-1383.
- [10] J. Remón, P. Arcelus-Arillaga, L. García, J. Arauzo, Production of gaseous and liquid bio-fuels from the upgrading of lignocellulosic bio-oil in sub- and supercritical water: Effect of operating conditions on the process, *Energy Conversion and Management*, 119 (2016) 14-36.
- [11] C.A. Fisk, T. Morgan, Y. Ji, M. Crocker, C. Crofcheck, S.A. Lewis, Bio-oil upgrading over platinum catalysts using in situ generated hydrogen, *Applied Catalysis A: General*, 358 (2009) 150-156.
- [12] J. Penninger, M. Rep, Reforming of aqueous wood pyrolysis condensate in supercritical water, *International Journal of Hydrogen Energy*, 31 (2006) 1597-1606.
- [13] J.A. Onwudili, P.T. Williams, Catalytic conversion of bio-oil in supercritical water: Influence of RuO<sub>2</sub>/γ-Al<sub>2</sub>O<sub>3</sub> catalysts on gasification efficiencies and bio-methane production, *Applied Catalysis B: Environmental*, 180 (2016) 559-568.
- [14] M. Saidi, F. Samimi, D. Karimipourfard, T. Nimmanwudipong, B.C. Gates, M.R. Rahimpour, Upgrading of lignin-derived bio-oils by catalytic hydrodeoxygenation, *Energy and Environmental Science*, 7 (2014) 103-129.
- [15] I. Gandarias, P.L. Arias, *Hydrotreating catalytic processes for oxygen removal in the upgrading of bio-oils and bio-chemicals*, 2013.
- [16] J. Zhu, A. Holmen, D. Chen, Carbon Nanomaterials in Catalysis: Proton Affinity, Chemical and Electronic Properties, and their Catalytic Consequences, *ChemCatChem*, 5 (2013) 378-401.
- [17] P. Serp, J.L. Figueiredo, *Carbon Materials for Catalysis*, 2008.
- [18] D.J.M. DeVlieger, D.B. Thakur, L. Lefferts, K. Seshan, Carbon nanotubes: A promising catalyst support material for supercritical water gasification of biomass waste, *ChemCatChem*, 4 (2012) 2068-2074.
- [19] J.K. Chinthaginjala, K. Seshan, L. Lefferts, Preparation and application of carbon-nanofiber based microstructured materials as catalyst supports, *Industrial and Engineering Chemistry Research*, 46 (2007) 3968-3978.
- [20] R.W. Gosselink, W. Xia, M. Muhler, K.P. de Jong, J.H. Bitter, Enhancing the activity of Pd on carbon nanofibers for deoxygenation of amphiphilic fatty acid molecules through support polarity, *ACS Catalysis*, 3 (2013) 2397-2402.
- [21] M.L. Toebes, T.A. Nijhuis, J. Hajek, J.H. Bitter, A.J. van Dillen, D.Y. Murzin, K.P. de Jong, Support effects in hydrogenation of cinnamaldehyde over carbon nanofiber-supported platinum catalysts: Kinetic modeling, *Chemical Engineering Science*, 60 (2005) 5682-5695.
- [22] T. Tang, C. Yin, N. Xiao, M. Guo, F.-S. Xiao, High activity in catalytic oxidation of benzyl alcohol with molecular oxygen over carboxylic-functionalized carbon Nanofiber-Supported Ruthenium Catalysts, *Catalysis Letters*, 127 (2008) 400-405.

- [23] R.T.K. Baker, K. Laubernds, A. Wootsch, Z. Paal, Pt/graphite nanofiber catalyst in n-hexane test reaction, *Journal of Catalysis*, 193 (2000) 165-167.
- [24] A. Chambers, T. Nemes, N.M. Rodriguez, R.T.K. Baker, Catalytic behavior of graphite nanofiber supported nickel particles. 1. Comparison with other support media, *Journal of Physical Chemistry B*, 102 (1998) 2251-2258.
- [25] C. Park, R.T.K. Baker, Catalytic behavior of graphite nanofiber supported nickel particles. 2. The influence of the nanofiber structure, *Journal of Physical Chemistry B*, 102 (1998) 5168-5177.
- [26] N.M. Rodriguez, M.S. Kim, R.T.K. Baker, Carbon nanofibers- A unique catalyst support medium, *Journal of Physical Chemistry*, 98 (1994) 13108-13111.
- [27] P. Serp, M. Corrias, P. Kalck, Carbon nanotubes and nanofibers in catalysis, *Applied Catalysis A: General*, 253 (2003) 337-358.
- [28] V. Brotons, B. Coq, J.M. Planeix, Catalytic influence of bimetallic phases for the synthesis of single-walled carbon nanotubes, *Journal of Molecular Catalysis A: Chemical*, 116 (1997) 397-403.
- [29] V. Lordi, N. Yao, J. Wei, Method for supporting platinum on single-walled carbon nanotubes for a selective hydrogenation catalyst, *Chemistry of Materials*, 13 (2001) 733-737.
- [30] J.M. Nhut, R. Vieira, L. Pesant, J.P. Tessonnier, N. Keller, G. Ehret, C. Pham-Huu, M.J. Ledoux, Synthesis and catalytic uses of carbon and silicon carbide nanostructures, *Catalysis Today*, 76 (2002) 11-32.
- [31] C. Pham-Huu, N. Keller, G. Ehret, L.J. Charbonniere, R. Ziessel, M.J. Ledoux, Carbon nanofiber supported palladium catalyst for liquid-phase reactions - An active and selective catalyst for hydrogenation of cinnamaldehyde into hydrocinnamaldehyde, *Journal of Molecular Catalysis A: Chemical*, 170 (2001) 155-163.
- [32] J.M. Planeix, N. Coustel, B. Coq, V. Brotons, P.S. Kumbhar, R. Dutartre, P. Geneste, P. Bernier, P.M. Ajayan, Application of carbon nanotubes as supports in heterogeneous catalysis, *Journal of the American Chemical Society*, 116 (1994) 7935-7936.
- [33] M.L. Toebes, F.F. Prinsloo, J.H. Bitter, A.J. van Dillen, K.P. de Jong, Influence of oxygen-containing surface groups on the activity and selectivity of carbon nanofiber-supported ruthenium catalysts in the hydrogenation of cinnamaldehyde, *Journal of Catalysis*, 214 (2003) 78-87.
- [34] J.L. Pinilla, H. Purón, D. Torres, I. Suelves, M. Millan, Ni-MoS<sub>2</sub> supported on carbon nanofibers as hydrogenation catalysts: Effect of support functionalisation, *Carbon*, 81 (2015) 574-586.
- [35] Y. Zhao, C.-H. Li, Z.-X. Yu, K.-F. Yao, S.-F. Ji, J. Liang, Effect of microstructures of Pt catalysts supported on carbon nanotubes (CNTs) and activated carbon (AC) for nitrobenzene hydrogenation, *Materials Chemistry and Physics*, 103 (2007) 225-229.
- [36] T.G. Ros, A.J. van Dillen, J.W. Geus, D.C. Koningsberger, Surface oxidation of carbon nanofibres, *Chemistry-a European Journal*, 8 (2002) 1151-1162.
- [37] R. Gao, C.D. Tan, R.T.K. Baker, Ethylene hydroformylation on graphite nanofiber supported rhodium catalysts, *Catalysis Today*, 65 (2001) 19-29.
- [38] J.L. Pinilla, H. Purón, D. Torres, S. De Llobet, R. Moliner, I. Suelves, M. Millan, Carbon nanofibres coated with Ni decorated MoS<sub>2</sub> nanosheets as catalyst for vacuum residue hydroprocessing, *Applied Catalysis B: Environmental*, 148-149 (2014) 357-365.
- [39] H. Purón, J.L. Pinilla, I. Suelves, M. Millan, Acid treated carbon nanofibers as catalytic support for heavy oil hydroprocessing, *Catalysis Today*, 249 (2015) 79-85.

- [40] M.C. Bahome, L.L. Jewell, D. Hildebrandt, D. Glasser, N.J. Coville, Fischer-Tropsch synthesis over iron catalysts supported on carbon nanotubes, *Applied Catalysis A: General*, 287 (2005) 60-67.
- [41] M.C. Bahome, L.L. Jewell, K. Padayachy, D. Hildebrandt, D. Glasser, A.K. Datye, N.J. Coville, Fe-Ru small particle bimetallic catalysts supported on carbon nanotubes for use in Fischer-Tropsch synthesis, *Applied Catalysis A: General*, 328 (2007) 243-251.
- [42] G.L. Bezemer, P.B. Radstake, U. Falke, H. Oosterbeek, H. Kuipers, A. van Dillen, K.P. de Jong, Investigation of promoter effects of manganese oxide on carbon nanofiber-supported cobalt catalysts for Fischer-Tropsch synthesis, *Journal of Catalysis*, 237 (2006) 152-161.
- [43] Z.J. Liu, Z.Y. Yuan, W.Z. Zhou, L.M. Peng, Z.D. Xu, Co/carbon-nanotube monometallic system: the effects of oxidation by nitric acid, *Physical Chemistry Chemical Physics*, 3 (2001) 2518-2521.
- [44] J.Z. Luo, L.Z. Gao, Y.L. Leung, C.T. Au, The decomposition of NO on CNTs and 1 wt% Rh/CNTs, *Catalysis Letters*, 66 (2000) 91-97.
- [45] J. Garcia, H.T. Gomes, P. Serf, P. Kalck, J.L. Figueiredo, J.L. Faria, Carbon nanotube supported ruthenium catalysts for the treatment of high strength wastewater with aniline using wet air oxidation, *Carbon*, 44 (2006) 2384-2391.
- [46] J. Garcia, H.T. Gomes, P. Serp, P. Kalck, J.L. Figueiredo, J.L. Faria, Platinum catalysts supported on MWNT for catalytic wet air oxidation of nitrogen containing compounds, *Catalysis Today*, 102 (2005) 101-109.
- [47] S.A. Channiwala, P.P. Parikh, A unified correlation for estimating HHV of solid, liquid and gaseous fuels, *Fuel*, 81 (2002) 1051-1063.
- [48] J.L. Pinilla, R. Utrilla, M.J. Lázaro, I. Suelves, R. Moliner, J.M. Palacios, A novel rotary reactor configuration for simultaneous production of hydrogen and carbon nanofibers, *Int. J. Hydrog. Energy*, 34 (2009) 8016-8022.
- [49] J. Remón, J.A. Medrano, F. Bimbela, L. García, J. Arauzo, Ni/Al-Mg-O solids modified with Co or Cu for the catalytic steam reforming of bio-oil, *Applied Catalysis B: Environmental*, 132-133 (2013) 433-444.
- [50] J.L. Pinilla, P. Arcelus-Arrillaga, H. Puro, M. Millan, Selective Catalytic Steam Cracking of anthracene using mesoporous Al<sub>2</sub>O<sub>3</sub> supported Ni-based catalysts doped with Na, Ca or K, *Applied Catalysis A: General*, 459 (2013) 17-25.
- [51] T.G. Ros, A.J. Van Dillen, J.W. Geus, D.C. Koningsberger, Surface oxidation of carbon nanofibres, *Chemistry - A European Journal*, 8 (2002) 1151-1162.
- [52] J.L. Figueiredo, M.F.R. Pereira, M.M.A. Freitas, J.J.M. Órfão, Modification of the surface chemistry of activated carbons, *Carbon*, 37 (1999) 1379-1389.
- [53] J. Matos, M. Rosales, G. González, C.U. de Navarro, Changes on texture and crystalline phase of activated carbon-supported Ni-Ca catalyst during dry methane reforming, *Open Materials Science Journal*, 4 (2010) 125-132.
- [54] W. Zhang, Y. Li, X. Zeng, S. Peng, Synergetic effect of metal nickel and graphene as a cocatalyst for enhanced photocatalytic hydrogen evolution via dye sensitization, *Scientific Reports*, 5 (2015).
- [55] M.C. Biesinger, B.P. Payne, A.P. Grosvenor, L.W.M. Lau, A.R. Gerson, R.S.C. Smart, Resolving surface chemical states in XPS analysis of first row transition metals, oxides and hydroxides: Cr, Mn, Fe, Co and Ni, *Applied Surface Science*, 257 (2011) 2717-2730.
- [56] R.L. Chin, D.M. Hercules, Surface spectroscopic characterization of cobalt-molybdenum-alumina catalysts, *Journal of Physical Chemistry*, 86 (1982) 3079-3089.

- [57] M.K. Van Der Lee, A. Van Jos Dillen, J.H. Bitter, K.P. De Jong, Deposition precipitation for the preparation of carbon nanofiber supported nickel catalysts, *Journal of the American Chemical Society*, 127 (2005) 13573-13582.
- [58] I. Kvande, G. Øye, N. Hammer, M. Rønning, S. Raaen, A. Holmen, J. Sjöblom, D. Chen, Deposition of Au colloids on plasmachemically modified carbon nanofibers, *Carbon*, 46 (2008) 759-765.
- [59] P. Duan, X. Bai, Y. Xu, A. Zhang, F. Wang, L. Zhang, J. Miao, Catalytic upgrading of crude algal oil using platinum/gamma alumina in supercritical water, *Fuel*, 109 (2013) 225-233.
- [60] P. Duan, P.E. Savage, Catalytic hydrotreatment of crude algal bio-oil in supercritical water, *Applied Catalysis B: Environmental*, 104 (2011) 136-143.
- [61] P. Duan, P.E. Savage, Catalytic treatment of crude algal bio-oil in supercritical water: optimization studies, *Energy & Environmental Science*, 4 (2011) 1447.
- [62] P. Duan, P.E. Savage, Upgrading of crude algal bio-oil in supercritical water, *Bioresource technology*, 102 (2011) 1899-1906.
- [63] J. Chaminand, L.a. Djakovitch, P. Gallezot, P. Marion, C. Pinel, C.c. Rosier, Glycerol hydrogenolysis on heterogeneous catalysts, *Green Chemistry*, 6 (2004) 359.
- [64] M. Guisnet, Characterization Of Acid Catalysts By Use Of Model Reactions, in: C.N.G.C.Y.B.T. B. Imelik, J.C. Vedrine (Eds.) *Studies in Surface Science and Catalysis*, Elsevier, 1985, pp. 283-297.
- [65] N. Mahmood, Z. Yuan, J. Schmidt, C. Xu, Depolymerization of lignins and their applications for the preparation of polyols and rigid polyurethane foams: A review, *Renewable and Sustainable Energy Reviews*, 60 (2016) 317-329.

## **FIGURE CAPTIONS**

**Fig. 1.** Schematic of the micro-bomb batch reactor.

**Fig. 2.** TEM micrographs of as-prepared CNF.

**Fig. 3.** CO (a) and CO<sub>2</sub> (b) profiles obtained by TPD.

**Fig. 4.** TEM micrographs of NiCo/CNFf (a), NiCo/CNFf-600 (b) and NiCo/CNFf-900 (c). The insets show the particle size distribution calculated from more than 400 nanoparticles. (d) EDX analysis of a single nanoparticle in NiCo-CNFf catalyst.

**Fig. 5.** Powder XRD patterns of CNF supported catalysts

**Fig. 6.** a) Ni 2p and b) Co 2p XPS spectra of CNF supported catalysts

## TABLES

*Table 1. Bio-oil characterisation results. Results are presented as mean  $\pm$  standard deviation.*

<b>Composition</b>	
Organics (wt.%)	60.95
Ashes (wt.%)	<0.001
H <sub>2</sub> O (wt.%)	39.05 $\pm$ 0.39
<b>Ultimate Analysis (raw basis)</b>	
C (wt.%)	32.86 $\pm$ 0.40
H (wt.%)	6.73 $\pm$ 0.16
O (wt.%) <sup>a</sup>	58.91 $\pm$ 0.48
N (wt.%)	0.51 $\pm$ 0.03
S (wt.%)	0.99 $\pm$ 0.11
<b>Physical properties</b>	
pH	2.45 $\pm$ 0.02
Density (g/mL)	1.16 $\pm$ 0.01
Viscosity (mPa·s)	10.44 $\pm$ 0.48
HHV (MJ/kg) estimated	13.40 $\pm$ 0.54
HHV (MJ/kg) estimated dry basis	17.34 $\pm$ 0.77
<b>Chemical Composition (Relative area %)</b>	
Ketones	18.22 $\pm$ 0.38
Carboxylic Acids	45.52 $\pm$ 2.42
Furans	3.71 $\pm$ 0.32
Alcohols	2.22 $\pm$ 0.35
Aldehydes	1.41 $\pm$ 0.32
Phenols	21.35 $\pm$ 1.19
Benzenes	3.86 $\pm$ 1.93
Sugars	1.99 $\pm$ 1.14
Nitrogen compounds	1.72 $\pm$ 0.51

<sup>a</sup> Determined by difference

Table 2. Response variables. Definitions and analytical techniques used in their determination.

Product	Response variable	Analytical method
Gas	Gas yield (%) = $\frac{\text{mass of gas (g)}}{\text{mass of dry bio - oil (g)}} 100$	Gas Chromatograph
	Composition (vol. %) = $\frac{\text{mol of each gas}}{\text{total mol of gas}} 100$	
	LHV (MJ/m <sup>3</sup> STP) = 0.1079 H <sub>2</sub> (vol.%) + 0.1263 CO (vol.%) + 0.3581 CH <sub>4</sub> (vol.%)	Estimated
Liquid	Liquid yield (%) = $\frac{\text{mass of upgrading bio - oil (g)}}{\text{mass of dry bio - oil (g)}} 100$	
	Composition (area %) = $\frac{\text{area of each compound}}{\text{total area}} 100$	GC-MS (Gas Chromatography-Mass Spectrometry).
	C, H, O (wt. %) = $\frac{\text{mass of C, H, O (g)}}{\text{mass of dry bio - oil (g)}} 100$	Elemental Analysis
	HHV (MJ/kg) = 0.3491 C (wt.%) + 1.1783 H (wt.%) - 0.1034 O (wt.%) - 0.015 N (wt.%) + 0.1005 S (wt.%)	Estimated
Solid	Solid yield (%) = $\frac{\text{mass of solid (g)}}{\text{mass of dry bio - oil (g)}} 100$	

Table 3. Crystallographic parameters calculated from XRD and textural properties determined by N<sub>2</sub> adsorption of the CNFs.

Sample	L <sub>c</sub> (nm)	d <sub>002</sub> (nm)	S <sub>BET</sub> (m <sup>2</sup> ·g <sup>-1</sup> )	V <sub>p</sub> (cm <sup>3</sup> ·g <sup>-1</sup> )	d <sub>p</sub> (nm)
CNF <sub>f</sub>	6.3	0.3409	97.0	0.286	14.1
CNF <sub>f-600</sub>	6.4	0.3413	99.5	0.3	14.2
CNF <sub>f-900</sub>	6.6	0.3415	95.6	0.296	14.2

d<sub>002</sub> and L<sub>c</sub> refer to the interlayer spacing and the mean crystallite size of the carbon structures, respectively. S<sub>BET</sub> is the specific surface area, V<sub>p</sub> the total pore volume and d<sub>p</sub> the average pore diameter calculated from the BJH model applied to the adsorption branch of the isotherms.

Table 4. Surface chemistry measured by TPD (total amount of CO and CO<sub>2</sub> released and total oxygen content) and XPS (surface oxygen content and surface oxygen to carbon ratio).

Sample	CO (mmol·g <sub>cat</sub> <sup>-1</sup> )	CO <sub>2</sub> (mmol·g <sub>cat</sub> <sup>-1</sup> )	Oxygen content TPD (%)	Oxygen content XPS (%)	(O/C) <sub>XPS</sub>
CNF <sub>f</sub>	0.65	0.169	1.6	7.5	0.081
CNF <sub>f</sub> -600	0.419	0.04	0.8	6.1	0.065
CNF <sub>f</sub> -900	0.248	0.029	0.5	5.5	0.058

Table 5. Crystallographic parameters calculated from XRD and textural properties determined by N<sub>2</sub> adsorption of CNF and functionalised CNF.

Sample	Ni (wt %)	Co (wt %)	d <sub>NP-XRD</sub> (nm)	d <sub>Ni-TEM</sub> (nm)	S <sub>BET</sub> (m <sup>2</sup> ·g <sup>-1</sup> )	V <sub>p</sub> (cm <sup>3</sup> ·g <sup>-1</sup> )	d <sub>p</sub> (nm)
NiCo/CNF <sub>f</sub>	17.4±0.2	2.7±0.06	21.1	23 ± 9.8	100.5	0.361	15.8
NiCo/CNF <sub>f</sub> -600	18.5±0.2	2.3±0.08	22.4	18.8 ± 9.1	95.1	0.308	14.7
NiCo/CNF <sub>f</sub> -900	16.7±0.2	2.1±0.08	19.1	19.8 ± 10.8	91.1	0.310	15.0

S<sub>BET</sub> is the specific surface area, V<sub>p</sub> the total pore volume and d<sub>p</sub> the average pore diameter calculated from the BJH model applied to the adsorption branch of the isotherms. Ni and Co were measured by ICP.

Table 6. Yields to gas, liquid (upgraded bio-oil) and solid. Results are expressed as mean ± standard error.

Catalyst	Gas yield (%)	Liquid yield (%)	Solid yield (%)
NiCo/CNF <sub>f</sub>	26.5±1.4 <sup>B</sup>	46.1±0.1 <sup>C</sup>	27.4±1.3 <sup>A</sup>
NiCo/CNF <sub>f</sub> -600	26.1±1.0 <sup>B</sup>	50.1±0.1 <sup>B</sup>	23.9±0.9 <sup>A,B</sup>
NiCo/CNF <sub>f</sub> -900	28.4±1.4 <sup>B</sup>	56.0±0.1 <sup>A</sup>	15.6±1.3 <sup>C</sup>
Blank	36.7±1.4 <sup>A</sup>	45.1±0.1 <sup>D</sup>	18.2±1.3 <sup>B,C</sup>

A, B, C and D are statistical homogeneous groups with 95% confidence  
Error has been calculated using a pooled estimate of error variance

Table 7. Composition (vol.%) and Lower Heating Value (LHV) of the gas phase. Results are expressed as mean  $\pm$  standard error.

Catalyst	H <sub>2</sub> (vol.%)	CO <sub>2</sub> (vol.%)	CO (vol.%)	CH <sub>4</sub> (vol.%)	LHV (MJ/STP m <sup>3</sup> )
NiCo/CNF <sub>f</sub>	17.8 $\pm$ 5.5 <sup>A</sup>	60.1 $\pm$ 9.8 <sup>A</sup>	13.7 $\pm$ 2.4 <sup>A</sup>	8.4 $\pm$ 1.7 <sup>A</sup>	6.7 $\pm$ 0.1 <sup>A</sup>
NiCo/CNF <sub>f</sub> -600	18.0 $\pm$ 3.9 <sup>A</sup>	60.9 $\pm$ 6.9 <sup>A</sup>	12.9 $\pm$ 1.7 <sup>A</sup>	8.2 $\pm$ 1.2 <sup>A</sup>	5.71 $\pm$ 0.1 <sup>A</sup>
NiCo/CNF <sub>f</sub> -900	15.5 $\pm$ 5.5 <sup>A</sup>	60.6 $\pm$ 9.8 <sup>A</sup>	16.0 $\pm$ 2.4 <sup>A</sup>	7.9 $\pm$ 1.7 <sup>A</sup>	6.5 $\pm$ 0.1 <sup>A</sup>
Blank	22.8 $\pm$ 5.5 <sup>A</sup>	56.4 $\pm$ 9.8 <sup>A</sup>	13.4 $\pm$ 2.4 <sup>A</sup>	6.4 $\pm$ 1.7 <sup>A</sup>	6.4 $\pm$ 0.1 <sup>A</sup>

A, B and C are statistical homogeneous groups with 95% confidence  
Error has been calculated using a pooled estimate of error variance

Table 8. Elemental Analysis (wt.%) and estimated HHV (MJ/kg) of the treated liquids and the original bio-oil. Results are expressed as mean  $\pm$  standard error.

Catalyst	C (wt.%)	H (wt.%)	O (wt.%)	S (wt.%)	H/C	O/C	HHV (MJ/kg)
NiCo/CNF <sub>f</sub>	72.1 $\pm$ 0.9 <sup>A</sup>	7.4 $\pm$ 0.1 <sup>A</sup>	19.8 $\pm$ 3.7 <sup>C</sup>	0.4 $\pm$ 0.1 <sup>A,B</sup>	0.102 $\pm$ 0.001 <sup>A</sup>	0.275 $\pm$ 0.02 <sup>C</sup>	31.9 $\pm$ 1.8 <sup>A</sup>
NiCo/CNF <sub>f</sub> -600	70.6 $\pm$ 0.6 <sup>A</sup>	7.1 $\pm$ 0.1 <sup>B</sup>	21.9 $\pm$ 2.6 <sup>C</sup>	0.3 $\pm$ 0.1 <sup>B</sup>	0.099 $\pm$ 0.001 <sup>A</sup>	0.310 $\pm$ 0.01 <sup>C</sup>	30.7 $\pm$ 1.3 <sup>A</sup>
NiCo/CNF <sub>f</sub> -900	57.8 $\pm$ 0.9 <sup>B</sup>	5.4 $\pm$ 0.1 <sup>C</sup>	36.2 $\pm$ 3.7 <sup>B</sup>	0.3 $\pm$ 0.1 <sup>B</sup>	0.093 $\pm$ 0.001 <sup>B</sup>	0.626 $\pm$ 0.02 <sup>B</sup>	22.8 $\pm$ 1.8 <sup>B</sup>
Blank	67.4 $\pm$ 0.9 <sup>A</sup>	7.0 $\pm$ 0.1 <sup>B</sup>	25.2 $\pm$ 3.7 <sup>C</sup>	0.3 $\pm$ 0.1 <sup>B</sup>	0.104 $\pm$ 0.001 <sup>A</sup>	0.374 $\pm$ 0.02 <sup>C</sup>	29.2 $\pm$ 1.8 <sup>A</sup>
Bio-oil *	53.9 $\pm$ 0.4 <sup>B</sup>	3.3 $\pm$ 0.2 <sup>D</sup>	41.3 $\pm$ 0.5 <sup>A</sup>	0.6 $\pm$ 0.1 <sup>A</sup>	0.062 $\pm$ 0.001 <sup>C</sup>	0.768 $\pm$ 0.01 <sup>A</sup>	18.5 $\pm$ 0.3 <sup>C</sup>

A, B, C and D are statistical homogeneous groups with 95% confidence  
Error has been calculated using a pooled estimate of error variance  
\* Bio-oil properties are expressed as mean  $\pm$  standard deviation

Table 9. GC-MS analysis of the treated liquids and the original bio-oil. Results are presented as the relative chromatographic area (%) of each family of compounds and expressed as mean  $\pm$  standard error.

Catalyst	Hydrocarbons	Alcohols	Carboxylic acids	Ketones	Phenols	Furans	Cyclic compounds
NiCo/CNF <sub>f</sub>	1.09 $\pm$ 6.91 <sup>A</sup>	1.93 $\pm$ 1.02 <sup>A</sup>	13.96 $\pm$ 2.32 <sup>B</sup>	9.94 $\pm$ 6.93 <sup>A</sup>	54.92 $\pm$ 8.55 <sup>A</sup>	4.30 $\pm$ 6.29 <sup>A</sup>	13.85 $\pm$ 1.53 <sup>B</sup>
NiCo/CNF <sub>f</sub> -600	9.28 $\pm$ 4.88 <sup>A</sup>	0.99 $\pm$ 0.72 <sup>A</sup>	13.83 $\pm$ 1.64 <sup>B</sup>	6.92 $\pm$ 4.89 <sup>A</sup>	36.57 $\pm$ 6.05 <sup>B</sup>	6.29 $\pm$ 4.45 <sup>A</sup>	26.88 $\pm$ 1.08 <sup>A</sup>
NiCo/CNF <sub>f</sub> -900	4.49 $\pm$ 6.91 <sup>A</sup>	0.0 <sup>A</sup>	9.10 $\pm$ 2.32 <sup>C</sup>	23.98 $\pm$ 6.93 <sup>A</sup>	53.88 $\pm$ 8.55 <sup>A</sup>	4.64 $\pm$ 6.29 <sup>A</sup>	2.47 $\pm$ 1.53 <sup>C</sup>
Blank	0.57 $\pm$ 6.91 <sup>A</sup>	0.0 <sup>A</sup>	18.90 $\pm$ 2.32 <sup>B</sup>	21.95 $\pm$ 6.93 <sup>A</sup>	51.92 $\pm$ 8.55 <sup>A</sup>	6.66 $\pm$ 6.29 <sup>A</sup>	0.00 $\pm$ 1.53 <sup>C</sup>
Bio-oil *	0.00 <sup>A</sup>	2.22 $\pm$ 0.35 <sup>A</sup>	45.52 $\pm$ 2.42 <sup>A</sup>	18.22 $\pm$ 0.38 <sup>A</sup>	21.35 $\pm$ 1.19 <sup>C</sup>	3.71 $\pm$ 0.32 <sup>A</sup>	0.00 <sup>C</sup>

A, B and C are statistical homogeneous groups with 95% confidence  
Error has been calculated using a pooled estimate of error variance. Negative areas are the consequence of the statistical analysis of the data (standard error), and a null area must be considered in those cases.  
\* Bio-oil concentration is expressed as mean  $\pm$  standard deviation

# FIG.S

Fig. 1

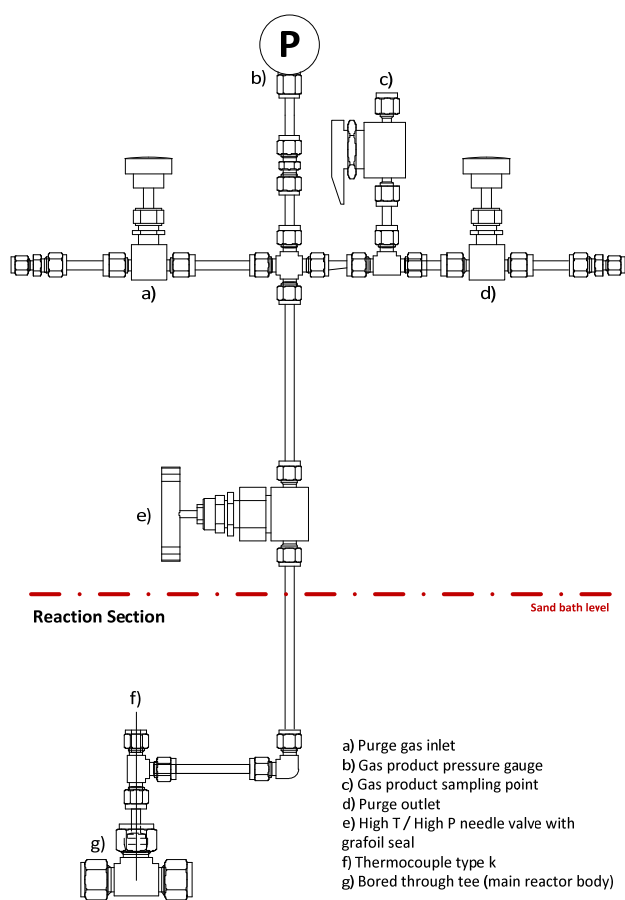


Fig. 2.

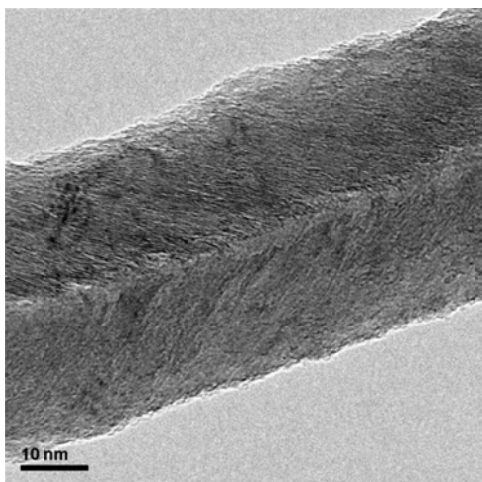
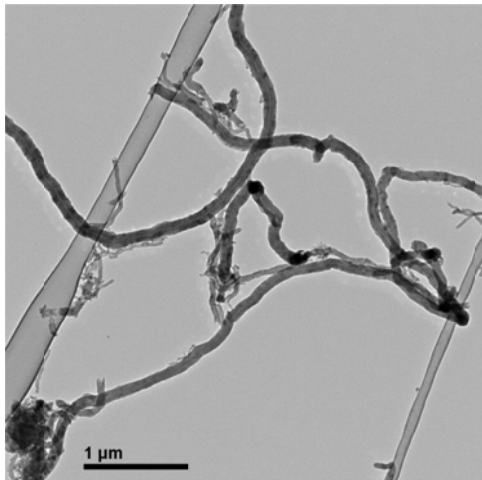


Fig. 3.

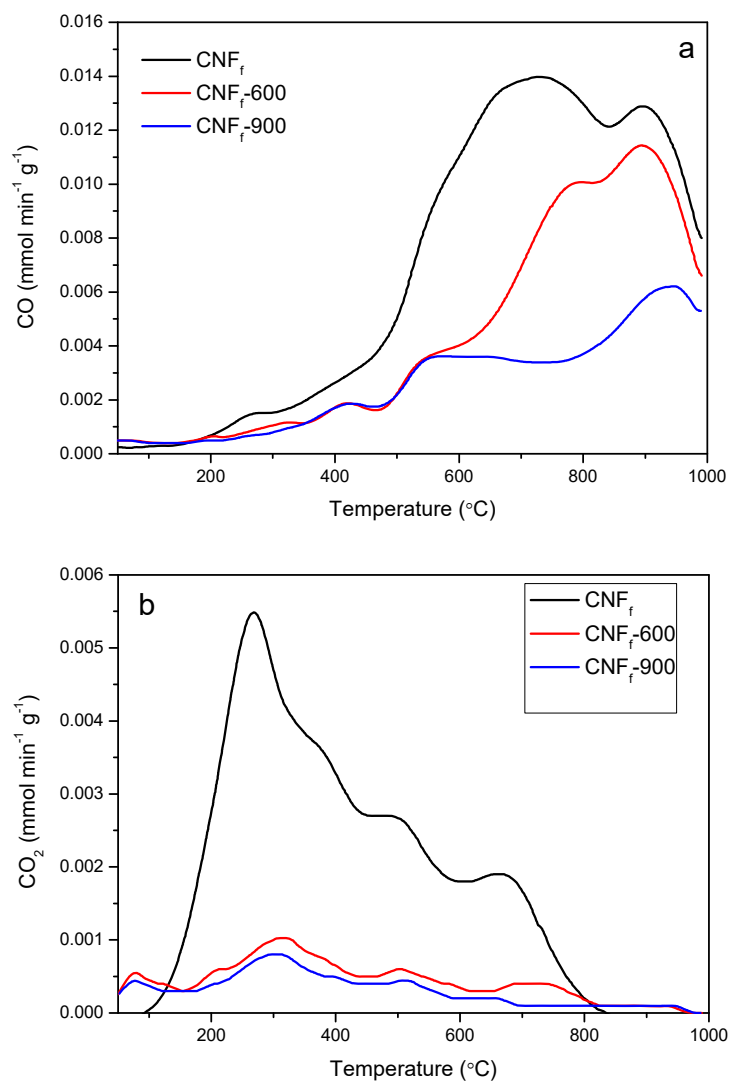
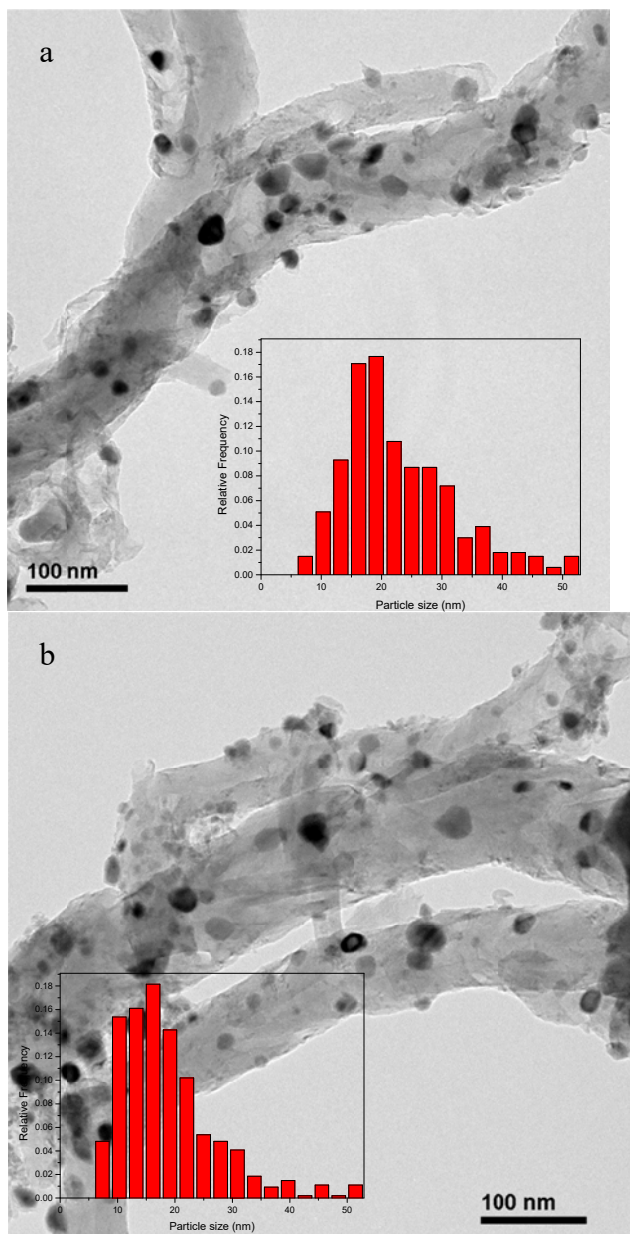


Fig. 4.



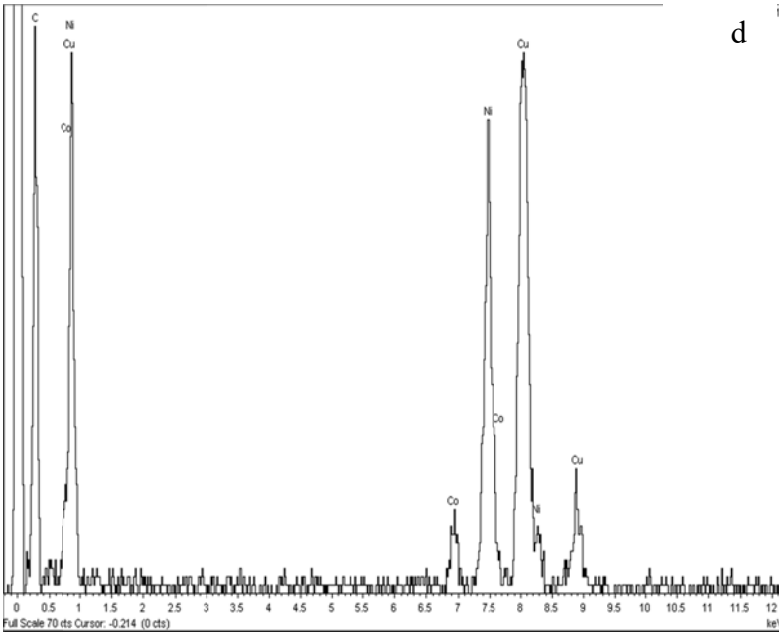
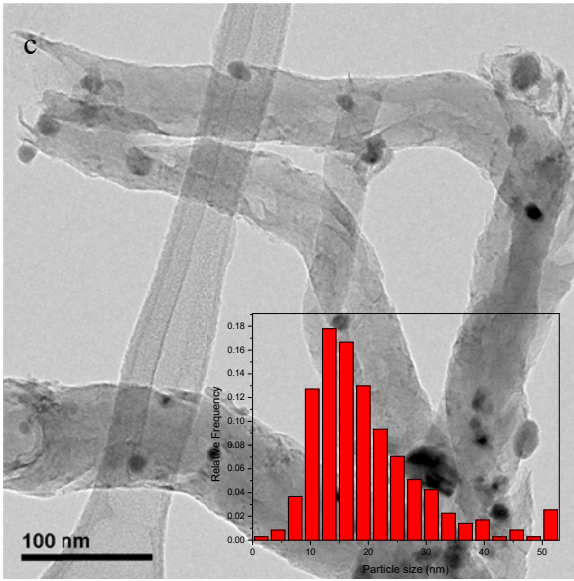


Fig. 5.

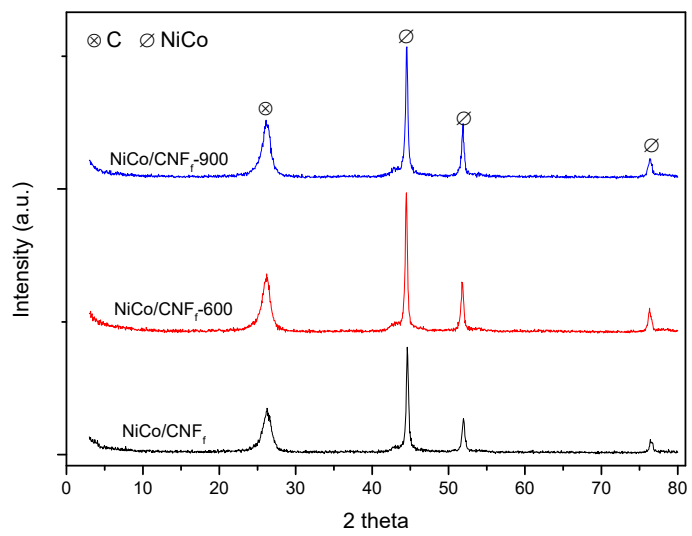


Fig. 6.

